

---

# ROBUST POLARIZATION GRADIENT COOLING OF TRAPPED IONS

---

Wenbing Li<sup>1,2\*</sup>, Sebastian Wolf<sup>1\*</sup>, Lukas Klein<sup>1</sup>, Dmitry Budker<sup>2,1,3,4</sup>,  
 Christoph E. Düllmann<sup>2,5,6,3</sup> and Ferdinand Schmidt-Kaler<sup>1,2</sup>

<sup>1</sup> QUANTUM, Institut für Physik, Johannes Gutenberg-Universität Mainz, 55128 Mainz, Germany

<sup>2</sup> Helmholtz-Institut Mainz, 55099 Mainz, Germany

<sup>3</sup> PRISMA Cluster of Excellence, Johannes Gutenberg-Universität Mainz, 55128 Mainz, Germany

<sup>4</sup> Department of Physics, University of California, Berkeley, CA 94720-7300, USA

<sup>5</sup> Department chemie, Johannes Gutenberg-Universität Mainz, 55128 Mainz, Germany

<sup>6</sup> GSI Helmholtzzentrum für Schwerionenforschung GmbH, 64291 Darmstadt, Germany

\* Authors to whom any correspondence should be addressed

wenbingli@uni-mainz.de

wolfs@uni-mainz.de

September 3, 2021

## ABSTRACT

We implement three-dimensional polarization gradient cooling of trapped ions. Counter-propagating laser beams near 393 nm impinge in  $\text{lin} \perp \text{lin}$  configuration, at a frequency below the  $S_{1/2}$  to  $P_{3/2}$  resonance in  $^{40}\text{Ca}^+$ . We demonstrate mean phonon numbers of 5.4(4) at a trap frequency of  $2\pi \times 285\text{kHz}$  and 3.3(4) at  $2\pi \times 480\text{kHz}$ , in the axial and radial directions, respectively. Our measurements demonstrate that cooling with laser beams detuned to lower frequencies from the resonance is robust against an elevated phonon occupation number, and thus works well for an initial ion motion far out of the Lamb-Dicke regime, for up to four ions, and for a micromotion modulation index  $\beta \leq 0.1$ . Still, we find that the spectral impurity of the laser field influences both, cooling rates and cooling limits. Thus, a Fabry-Pérot cavity filter is employed for efficiently suppressing amplified spontaneous emission of the diode laser.

**Keywords** Trapped ions · Laser cooling · Sub-Doppler cooling · Polarization gradient cooling

## 1 Introduction

Laser-cooled trapped ions are widely used in quantum simulation [1, 2, 3] and quantum computation [4, 5, 6], for high-performance optical clocks [7, 8, 9, 10] or precision spectroscopy [11, 12, 13, 14]. For those applications, Coulomb crystals are formed under Doppler cooling [15, 16, 17]. However, in order to improve the fidelity of quantum gate operations in an ion-based quantum computer, to reduce systematic errors in an optical ion clock, and in precision spectroscopy applications, one may require deeper cooling of the ion degrees of motion, including collective modes in the ion crystal.

Nearly perfect ground state cooling is routinely achieved by resolved sideband (SB) cooling techniques which either employ a narrow dipole-forbidden transition [18, 19, 20] or Raman transitions between hyperfine or Zeeman ground state levels [21, 22, 23]. For a crystal of  $N$  ions, the number of collective modes is  $3N$  such that sequentially cooling on all resolved sidebands becomes increasingly impractical for large  $N$ . However, the spectral lineshape of a three-level system may be tailored by electromagnetically induced transparency (EIT) such that multiple collective modes

are cooled simultaneously [24, 25, 26, 27]. This bandwidth of cooling - well suited to cool a collection of collective modes - may be further increased in the polarization gradient cooling (PGC) method. In the pioneering theoretical work by C. Cohen-Tannoudji and co-workers [28, 29], sub-Doppler PGC experimental results on atomic ensembles obtained by S. Chu and W. D. Phillips were explained, for which all three were awarded the Physics Nobel prize in 1997 [30, 31, 32]. Also for trapped ions, sub-Doppler cooling was proposed [33, 34] and led to first experiments by PGC [35]. Only recently, PGC was demonstrated for a single trapped ion in three dimensions, and for small linear crystals [36], highlighting the large cooling bandwidth of this method. PGC was extended to linear ion crystals with up to 51 ions and 2D-crystals in zig-zag configuration with 22 ions [37].

The most appealing application of PGC is sub-Doppler multi-mode cooling over a large band of motional frequencies. The PGC cooling bandwidth exceeds that of EIT cooling, therefore leading to a fast reduction of phonon numbers even for a large number of vastly different mode frequencies, significantly below Doppler cooling limits. In this work, we aim for robust sub-Doppler cooling for trapped ions far outside the Lamb-Dicke regime (LDR), therefore, we chose a PGC-scheme with the laser frequency below resonance of the dipole transition (referred to as “red detuning”)  $S_{1/2} \leftrightarrow P_{3/2}$  near 393 nm in singly charged  $^{40}\text{Ca}^+$ . In this way parasitic Doppler heating is reduced during PGC. This might be especially important for fast PGC with light detuned by only a few linewidths from the  $2\pi \times 23$  MHz dipole transition. Such robust PGC may be advantageous in case of non-ideal Doppler precooling or if the ions are exposed to strong heating events. We see an application case for externally generated (exotic) ions, injected into a Paul trap, captured and then sympathetically cooled down and incorporated into a laser-cooled host ion crystal. Specifically, we aim for precision spectroscopy of injected ions of various thorium isotopes and the low-energy isomer in  $^{229}\text{Th}$  [38, 39, 40, 41].

The paper is organized as follows: We start describing the PGC scheme in Sec. 2 and the ion trap and laser experimental setup in Sec. 3, and then present the PGC cooling results for a single ion and for a 4-ion linear crystal in Sec. 4. Furthermore, we study the robustness of PGC in typically encountered experimental situations such as excessively high initial phonon occupation number, an imperfect localization of the ion position at the trap center, and laser sources for PGC with spectral impurity in Sec. 5. This results demonstrate PGC as a versatile method for preparing ions in low axial and radial vibrational states.

## 2 Levels and transitions for polarization gradient cooling in $^{40}\text{Ca}^+$

Levels and relevant transitions in  $^{40}\text{Ca}^+$  are shown in Fig. 1 (a) and the most important transition for PGC near 393 nm with its Zeeman components in Fig. 1 (b). The dipole-allowed transition from  $S_{1/2}$  to  $P_{3/2}$  is excited off-resonantly by a pair of counter-propagating 393 nm beams in  $\text{lin} \perp \text{lin}$  configuration, forming thus a periodically varying spatial polarization gradient lattice along this direction with alternating  $\sigma^+, \pi, \sigma^-, \pi, \dots$  etc. polarization. If the frequency is red detuned relative to the  $S_{1/2}$  to  $P_{3/2}$  transition by  $\Delta$ , the variation of the Clebsch-Gordan coefficients leads to a periodically varying ac-Stark shift of the ground state Zeeman sublevels [30, 32], as shown in Fig. 1 (c). If the ion moves along the direction of this lattice, predominantly either  $m_J = +1/2 \leftrightarrow m_J = +3/2$  or  $m_J = -1/2 \leftrightarrow m_J = -3/2$  transitions are alternately excited, in spatial regions with polarization of either  $\sigma^+$  or  $\sigma^-$ , respectively. From the combination of ac-light shift and optical pumping, the ion will lose kinetic energy when climbing a potential hill. The wave vectors of the PGC beams are parallel with the magnetic field  $B$ . Its projections with the trap directions  $(x, y, z)$  have angles  $(60^\circ, 60^\circ, 45^\circ)$  as shown in Fig. 1 (d). Thus, in this setting PGC is acting in all three dimensions, and cools axial and radial modes of vibration. The magnetic field strength of  $\approx 343 \mu\text{T}$  is supplied with a set of permanent magnets which defines the quantization axis and leads to a splitting of  $2\pi \times 9.343$  MHz between the two Zeeman sublevels of the  $S_{1/2}$  manifold.

Calcium atoms evaporated from an oven are photoionized resonantly in two step scheme with beams at wavelength of 423 nm and 375 nm and captured in the trap. For Doppler cooling, 397 nm light is red detuned from the dipole-allowed  $S_{1/2}$  to  $P_{1/2}$  transition by  $\Delta \simeq -0.5\Gamma$ . Pumping out of the metastable D states is accomplished with beams near 866 nm and 854 nm. A beam near 729 nm is aligned parallel to the magnetic field direction and used for resolved sideband spectroscopy driving the narrow quadrupole  $|S_{1/2}, m_J = 1/2\rangle \leftrightarrow |D_{5/2}, m_J = 3/2\rangle$  transition for revealing the ion phonon mode occupation numbers.

## 3 Experimental setup and procedures

We designed and built a linear Paul trap with blade-shaped RF (radio frequency) and DC (static voltage) electrodes which are integrally machined out of one piece of stainless-steel. The RF electrodes feature a distance of 2 mm from the trap center. We operate the trap at RF frequency  $\Omega = 2\pi \times 5.83$  MHz with a peak-to-peak amplitude of 550 V to the RF pair of electrodes and generate trap frequencies of  $(\omega_x, \omega_y) = 2\pi \times (483, 480)$  kHz for the two radial directions. The

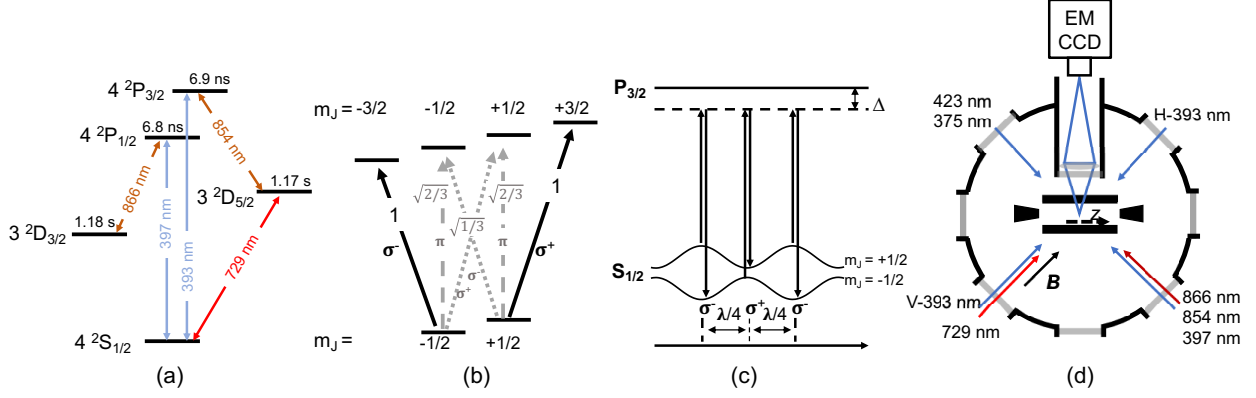


Figure 1: (a) Levels and relevant transitions and lifetimes in  $^{40}\text{Ca}^+$ . (b) Energy levels and transitions involved in PGC. A static magnetic field yields a Zeeman splitting of  $2\pi \times 9.343\text{ MHz}$  in the ground  $S_{1/2}$  state. The Clebsch-Gordan coefficients are shown for the transitions indicated with arrows. (c) Spatially varying light polarization results in position-dependent light shifts. The frequency of the PGC laser beams near 393 nm is detuned by  $\Delta$  from the  $S_{1/2} \leftrightarrow P_{3/2}$  transition, and the wave vector  $\mathbf{k}$  of both counter-propagating beams is aligned parallel to the magnetic field. (d) Geometry of trap, laser beams and magnetic field  $\mathbf{B}$ . The counter-propagating PGC beams are polarized horizontally (H-) and vertically (V-). Laser beams near 423 nm and 375 nm serve for photoionization loading, laser beams near 397 nm, 866 nm, 854 nm are used for Doppler cooling, and the ion fluorescence is imaged on a EMCCD camera. Light tuned near 729 nm is employed for resolved sideband spectroscopy.

DC pair is grounded, or kept at a small ( $<10\text{ V}$ ) voltage lifting further the degeneracy between radial trap frequencies. The axial confinement is provided by two end-cap electrodes at 14 mm distance. For a DC voltage of  $+800\text{ V}$ , an axial frequency  $\omega_z = 2\pi \times 220\text{ kHz}$  is created along the z-direction of the trap.

The laser system used in the experiment includes external-cavity diode lasers<sup>1</sup> operating near 397 nm for Doppler cooling, 866 nm and 854 nm for repumping, and 393 nm for PGC lattice. In addition, 729 nm light for probing the narrow quadrupole transition is supplied with a DL TA pro (Tapered Amplifier) locked to a high finesse optical cavity via Pound-Drever-Hall (PDH) resulting in a short-term frequency instability of  $\leq 100\text{ Hz}$ . The laser beams are switched by acousto-optic modulators (AOMs) operated in double pass configuration. All laser beams are coupled to the setup via polarization-maintaining single-mode fibers to ensure alignment stability. Laser-induced ion fluorescence is collected with a lens and imaged at a magnification of  $\approx 11.3$  onto an electron multiplying charge-coupled device (EMCCD) camera.

We investigate PGC with the following experimental sequence. First, the Ca ions are Doppler cooled with 397 nm laser light for 5 ms. The repumping light at 866 nm is switched on during Doppler cooling to prevent accumulation of ions in the  $D_{3/2}$  state. Second, the PGC laser beams at 393 nm are applied to the ions at orthogonal linear polarization and along the magnetic field. The two beams have a frequency difference of 50 kHz to create a moving polarization gradient. This is needed so that all ion wave packets experience a significant polarization gradient lattice at some point during the PGC period. This should not be necessary for ion wave packets that are larger than a period of the gradient; our experimental situation corresponds to the borderline of this regime. The intensity of the two 393 nm laser beams are calibrated with the fluorescence intensity detected with the EMCCD camera. During a PGC period, the light at 866 nm and at 854 nm is switched on to pump the populations out of the  $D_{3/2}$  and  $D_{5/2}$  states. Third, the ions are prepared in the  $|S_{1/2}, m_J = 1/2\rangle$  state via frequency-resolved optical pumping on the  $|S_{1/2}, m_J = -1/2\rangle \leftrightarrow |D_{5/2}, m_J = 1/2\rangle$  transition by a laser pulse at 729 nm combined with light at 854 nm. Finally, the motional state is probed by addressing the carrier and first-order sideband of the  $|S_{1/2}, m_J = 1/2\rangle \leftrightarrow |D_{5/2}, m_J = 3/2\rangle$  transition with a 729 nm laser pulse. At the end, the quantum state is read out for all individual ions via spatially resolved fluorescence detection at 397 nm recorded with the EMCCD camera.

## 4 Experimental characterization of PGC

Three dimensional PGC is compared to Doppler cooling on a single  $\text{Ca}^+$  ion by sideband spectroscopy of the  $|S_{1/2}, m_J = 1/2\rangle \leftrightarrow |D_{5/2}, m_J = 3/2\rangle$  transition, as shown in Fig. 2. In this measurement, the 393 nm laser light is

<sup>1</sup>All lasers are TOPTICA DL pro.

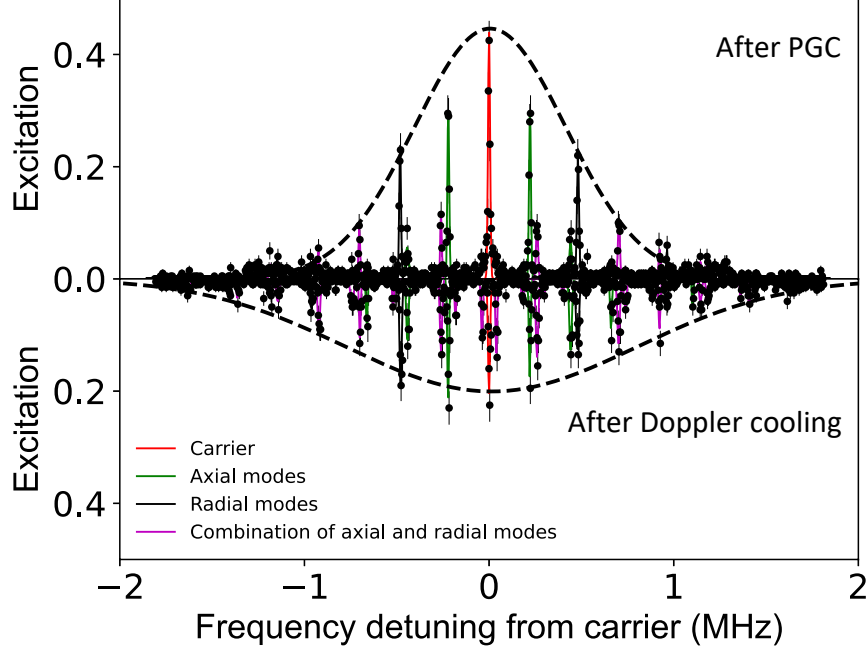


Figure 2: Spectroscopy of motional states. The  $|S_{1/2}, m_J = 1/2\rangle \leftrightarrow |D_{5/2}, m_J = 3/2\rangle$  transition is probed with a laser pulse at 729nm after PGC (top) and after Doppler cooling (bottom). Each experimental point (black solid circles) is the average of 200 measurements. The envelope fit (dashed black lines) include all the sidebands by taking into account the maxima of Gaussian fits to the carrier transition (red), axial sidebands (green), radial sidebands (black solid line) and combinations of axial and radial sidebands (magenta).

red-detuned by  $2\pi \times 180$  MHz, as determined with a wavelength meter<sup>2</sup>. The sideband data are fitted with individual Gaussian profiles. The higher-order sidebands involving the axial and radial motional modes and the higher order sidebands are considerably suppressed for the PGC case. Furthermore, a Gaussian envelope fit to the sideband amplitudes reveals a linewidth for the PGC case reduced by a factor of 1.92(6) compared to that with Doppler cooling.

To investigate the robustness of the presented PGC method, we initialize the ion with high initial phonon number occupation ( $> 4000$  phonons) by artificially deteriorating Doppler cooling via detuning the 397 nm light close to resonance ( $\Delta \ll \Gamma$ ) of the  $S_{1/2}$  to  $P_{1/2}$  transition. The cooling results compared with PGC after optimal Doppler cooling are shown in Fig. 3. With sufficient cooling time, identical final mean phonon numbers can be achieved independent of the initial ion temperature. For a detuning of  $2\pi \times 180$  MHz, the equilibrium cooling time is more than twice as long for high initial phonon numbers as for low initial phonon numbers. The PGC time can be reduced by decreasing the detuning of PGC light to  $2\pi \times 80$  MHz, which in turn increases the scattering rate of PGC light. We have also realized PGC for detunings as small as 30 MHz, and this was decreasing the cooling time to  $\leq 35 \mu\text{s}$  at the price of an elevated mean phonon number. For red-detuned PGC, we can explore the cross-over to Doppler cooling.

For three-dimensional PGC, residual micromotion is detrimental, especially for weak radial trap potentials. Therefore, we also investigate the influence of micromotion on PGC by adjusting micromotion-compensation voltages. The micromotion modulation index  $\beta$  is determined from the ratio of the excitation strength at the carrier and the micromotion-sideband frequency. We find PGC to be robust against residual micromotion corresponding to a range where the micromotion-compensation DC voltage is changed by 1.6 V (corresponding to a displacement of 560(35) nm from the trap center) and thus a micromotion-modulation index  $\beta \leq 0.1$ , see Fig. 4. However, micromotion is a decisive factor for three dimensional PGC. PGC light heats the ion instead of cooling once the micromotion is not compensated in a proper range.

We extend PGC to a 4-ion linear crystal confined in a trap potential, where the radial trap frequencies degeneracy is lifted by applying 3.0V on the DC electrode pair. The trap frequencies are  $(\omega_x, \omega_y, \omega_z) = 2\pi \times (427, 505, 190)$  kHz. We determine the axial phonon number by measuring Rabi oscillations on the  $S_{1/2} \leftrightarrow D_{5/2}$  transition. The Rabi oscillations of all four ions on the carrier transition are recorded individually to demonstrate the improved cooling of PGC with respect to Doppler cooling as shown in Fig. 5. For the Doppler-cooled ion crystal, no Rabi oscillations are

<sup>2</sup>WS7, HighFinesse

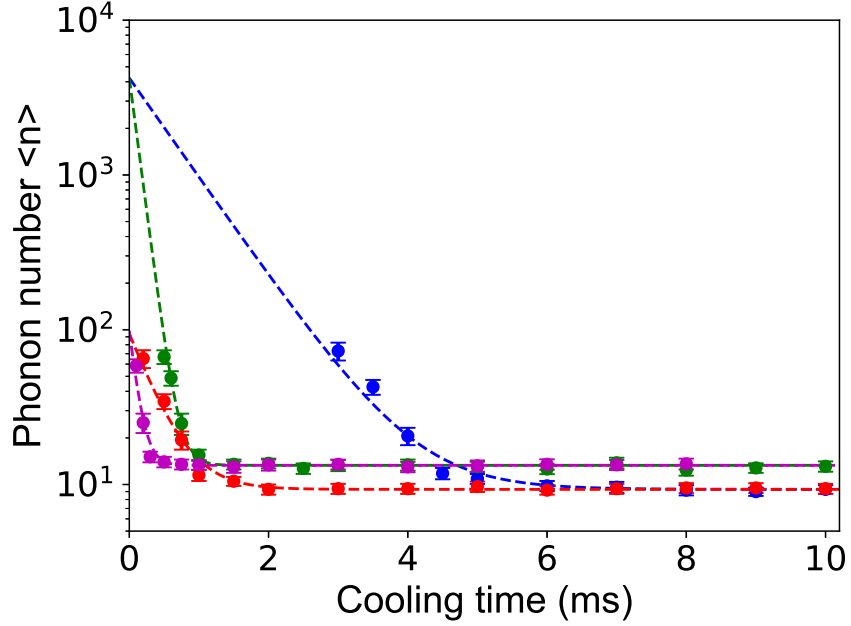


Figure 3: PGC performance for different cooling times and different initial phonon numbers. The initial state is prepared by Doppler cooling, which is either optimized or deliberately spoiled by tuning the Doppler cooling light close to resonance ( $\Delta \ll \Gamma$ ). The characteristic cooling times are  $\lesssim 7.0$ ms (blue circles fit with dashed line) and  $\lesssim 1.5$ ms (green) and the final mean phonon numbers 9.3(7) and 13.3(11), for PGC-light detuning of  $2\pi \times 180$ MHz and  $2\pi \times 80$ MHz, respectively. With low initial phonon numbers, the cooling times are decreased to  $\lesssim 3.0$ ms (red) and  $\lesssim 0.75$ ms (magenta), respectively.

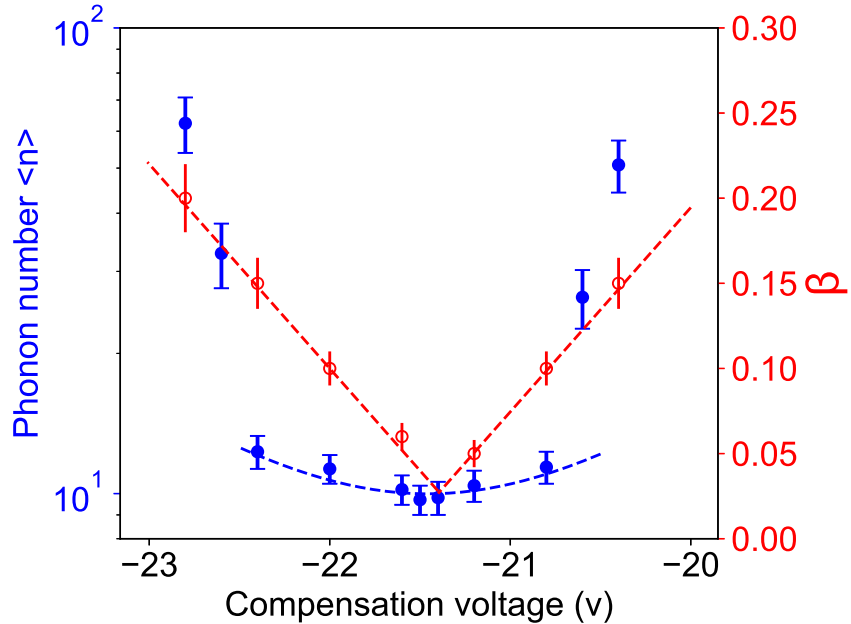


Figure 4: Mean phonon numbers (blue solid circles at left y-axis) and transition coupling strength on the micromotion (MM) sideband (red hollow circles at right y-axis) for different compensation voltages in one of the radial directions. The performance of PGC drops significantly for a modulation index  $\beta > 0.1$ .

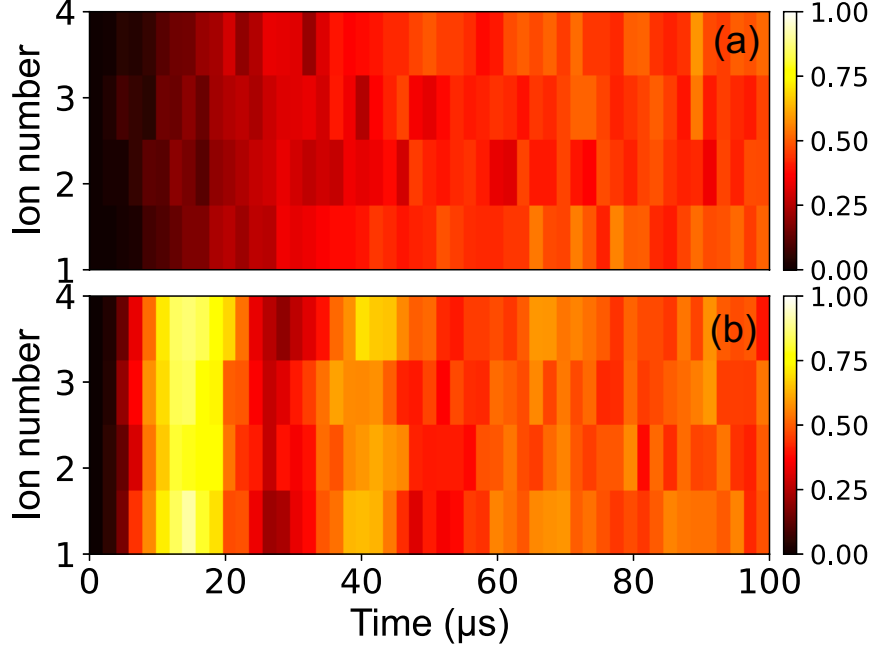


Figure 5: Rabi dynamics for a 4-ion linear crystal recorded individually on the carrier transition with an axial trap frequency of 190kHz. For Doppler cooled ions (a), no oscillations are visible, while they can clearly be observed after PGC (b).

visible for low trap frequencies, as shown in Fig. 5 (a). This is due to the averaging of Rabi oscillations for different phonon numbers. However, for the PGC case, Rabi oscillations can be observed, see Fig. 5 (b). Since all motional modes contribute to the Rabi dynamics of the carrier transition, this result indicates a low phonon occupation number ( $\eta^2 \langle n \rangle \ll 1$ , with the Lamb-Dicke parameter  $\eta$ ) for each motional mode of the 4-ion linear crystal.

The individual motional modes of the 4-ion linear crystal are investigated with spatially resolved sideband spectroscopy, as shown in Fig. 6. All the sidebands including center-of-mass (COM) and breathing modes of four ions can be distinctly resolved after PGC as shown in Fig. 6 (a)-(e). In contrast, for the Doppler cooled case shown in Fig. 6 (f) the high phonon numbers for each motional mode, and therefore the emergence of higher harmonics, prevent the resolution of individual sidebands. The final mean phonon number of the axial mode is evaluated as 12.5(7) after PGC by measuring Rabi oscillations of the carrier transition and the first axial sidebands of the COM mode of the inner ions.

## 5 Technique for improving PGC efficiency

An external-cavity diode laser is used for PGC in this work. In this case, resonant scattering events due to the amplified spontaneous emission (ASE) of the laser diode represent an additional heating source. The final temperature after PGC would be limited by this effect, especially if the frequency detuning is increased in order to approach the theoretical temperature limit [32, 37]. For large detunings, the lower cooling rate will be surpassed by the heating rate of the ASE background. To investigate this regime, we use a Fabry-Pérot cavity to purify the laser spectrum. Two mirrors with reflectivity of 99(1)% are spaced by 8 cm to form an optical resonator with a free spectral range (FSR) of 1.87 GHz and a finesse of about  $\mathcal{F} = 310$ . The resulting cavity filter with linewidth  $\Delta\nu \approx 6$  MHz, consequently, is able to sufficiently suppress spectral impurities of the laser light.

In an ideal case, the final mean phonon number is expected to be  $\langle n_0(\xi) \rangle = \xi + 1/(4\xi) - 1/2$  for a single ion [37], where  $\xi = s\Delta/(3\omega_z)$  is a dimensionless parameter,  $\Delta$  is the frequency detuning of 393 nm light, and  $\omega_z$  is the trap frequency in the axial direction. The saturation parameter is defined as  $s = \frac{\Omega^2/2}{\Gamma^2/4 + \Delta^2}$ , with  $\Gamma = 2\pi \times 23$  MHz the width of the excited state  $P_{3/2}$  and  $\Omega$  the Rabi frequency. To investigate how well we approach this limit using light with purified spectrum we measure the final mean phonon number for different frequency detunings of the 393 nm light with fixed power. For this experiment, the trap frequencies are  $(\omega_x, \omega_y, \omega_z) = 2\pi \times (483, 480, 285)$  kHz. Figure 7 shows the results with (red) and without (blue) cavity filter, respectively, and the theory fit with the laser intensity as the free

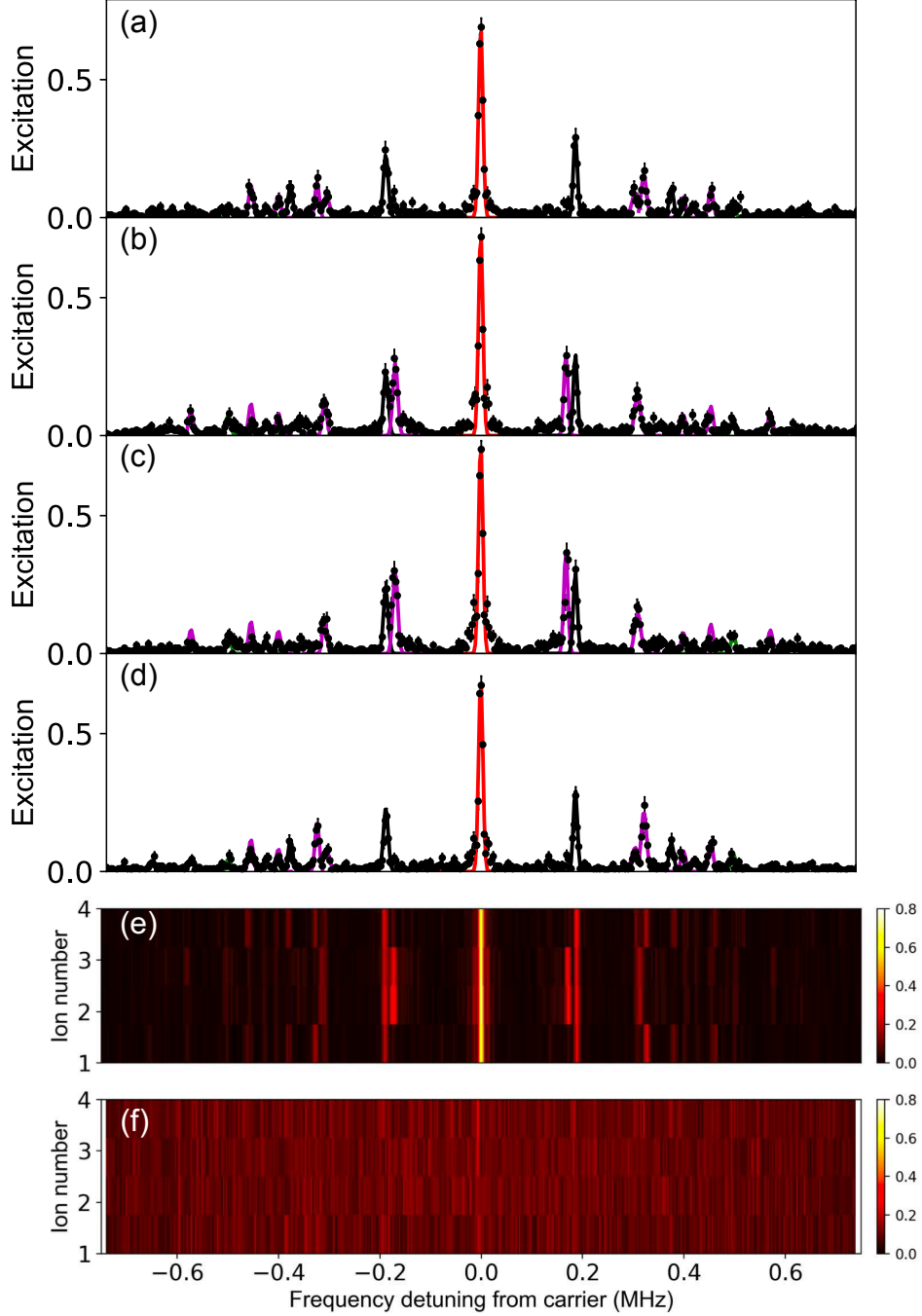


Figure 6: Sideband spectra of a 4-ion linear crystal. Each experimental point (black solid circles) is the average of 200 measurements. Sideband spectra after PGC ((a)-(d)) are fit with Gaussian profile, including the carrier (red line), the first axial modes (black lines), the COM modes, and breathing modes (magenta lines) for individual ions, and the sideband spectra after PGC (e) and after Doppler cooling (f), respectively. In the Doppler-cooled case, the individual sidebands cannot be clearly resolved.

parameter. Suggests that theoretical estimation a minimum mean phonon number of  $1/2$  can be achieved for  $\xi = 1/2$  when the optical well depth ( $2s\Delta/3$ ) equals the trap frequency  $\omega_z$ . From our measurement, the phonon number is in agreement with the theory prediction for  $\xi > 5$ . However, the minimum phonon number  $1/2$  predicted by the theory cannot be reached in our experiment since the trap potential is weak. Indeed, when the detuning is decreased to reduce the optical potential closer to the theoretical optimum, the optical pumping rate also decreases and, eventually, PGC

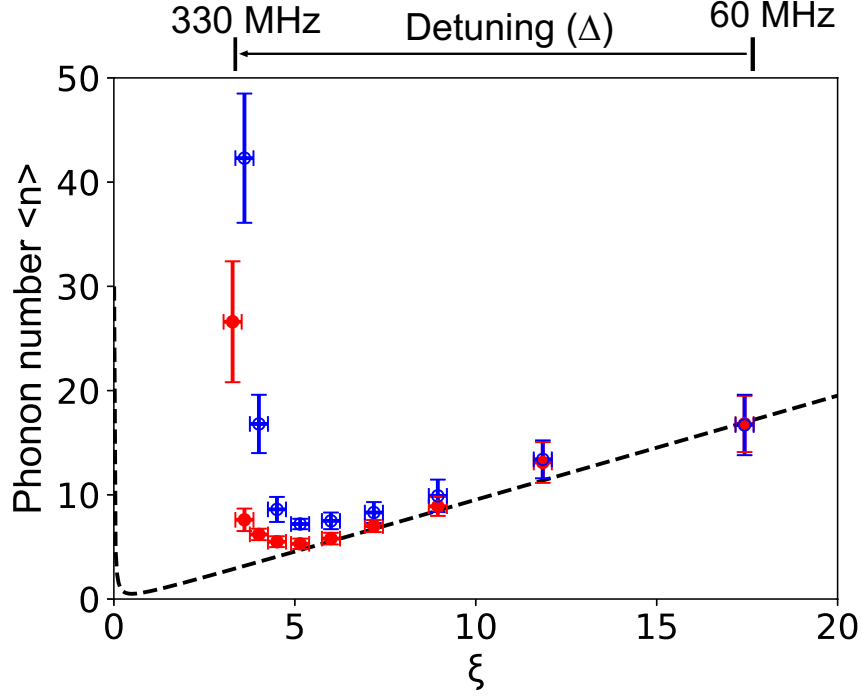


Figure 7: Mean phonon number after PGC for different  $\xi = s\Delta/(3\omega_z)$ , realized by changing the detuning  $\Delta$  with (red solid circles) and without (blue hollow circles) spectral purification via the cavity filter, respectively. The minimum mean phonon number at a detuning of  $2\pi \times 210$  MHz is reduced by 2.0(3) phonons.

cannot counteract the trap heating rate. At the frequency detuning of  $2\pi \times 210$  MHz, the minimal achieved phonon number is reduced by 2.0(3) when using the cavity filter.

To further investigate the effect of the ASE, we measure the cooling dynamics of PGC with and without cavity filter with a fixed frequency detuning of  $2\pi \times 210$  MHz and fixed intensity, see Fig. 8. The observed cooling time is improved by a factor of 2.1(2). To investigate the resonant scattering rate caused by the ASE we measured the pumping time from the  $m_J = +1/2$  Zeeman state to the equilibrium distribution in the ground  $S_{1/2}$  state, as follows. After Doppler cooling, the ion is prepared in the  $|S_{1/2}, m_J = +1/2\rangle$  ground state via optical pumping with 729 nm and 854 nm laser light. Afterwards, the 393 nm laser is applied to the ion with a varying duration resulting in partial population of the  $|S_{1/2}, m_J = -1/2\rangle$  level. Finally, the population in the  $|S_{1/2}, m_J = +1/2\rangle$  state is shelved to the  $D_{5/2}$  level with a 729 nm laser pulse and the residual population in the  $|S_{1/2}, m_J = +1/2\rangle$  state is detected by a fluorescence measurement. By scanning the pulse duration of the 393 nm laser light, the time to reach an equilibrium between the Zeeman ground states is measured for different frequency detunings as shown in the inset of Fig. 8. The increased equilibration time when the cavity filter is used compared with the case without the cavity filter is a result of reduced ASE background of the diode laser leading to a decreased resonant scattering rate. The suppression of the ASE background of the diode laser by the Fabry-Pérot cavity filter results in a reduced additional heating rate and, therefore, an improved cooling rate and final mean phonon number after PGC. The cavity-filter technique provides an option to improve PGC, even with diode lasers with excessive ASE.

To test whether the ultimate PGC performance would be limited by the heating rate of the trap, we evaluate heating in the axial motional mode. The final mean phonon number is measured for different waiting times after PGC. A linear fit to the data in Fig. 9 reveals a heating rate of 4.1(8) phonons per second at an axial trap frequency of  $2\pi \times 285$  kHz. This rate is of the same order of magnitude as the cooling rate close to final temperatures at the detuning of  $2\pi \times 210$  MHz and contributes to the limitation in achievable final mean phonon number of PGC.

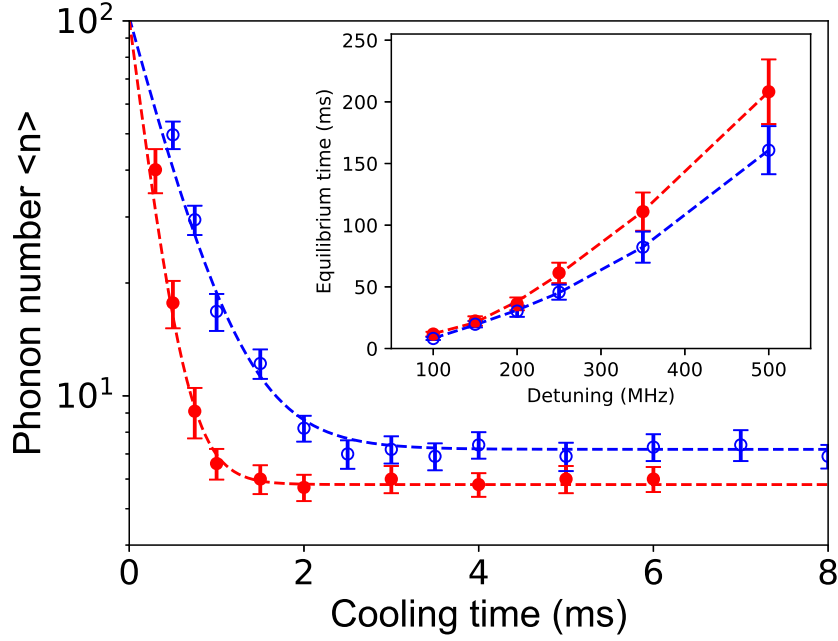


Figure 8: Cooling dynamics of PGC with (red solid circles) and without (blue hollow circles) cavity filter for fixed detuning of  $2\pi \times 210\text{MHz}$  and fixed intensity of the laser beams. The equilibrium cooling rate is improved by a factor of 2.1(2) when the cavity filter is used. Inset: pumping dynamics from one  $S_{1/2}$  Zeeman state to the equilibrium by the 393 nm light beams with (red solid circles) and without (blue hollow circles) cavity filter, respectively. The increased pumping rate without the cavity filter is caused by additional resonant scattering events due to the amplified spontaneous emission background.

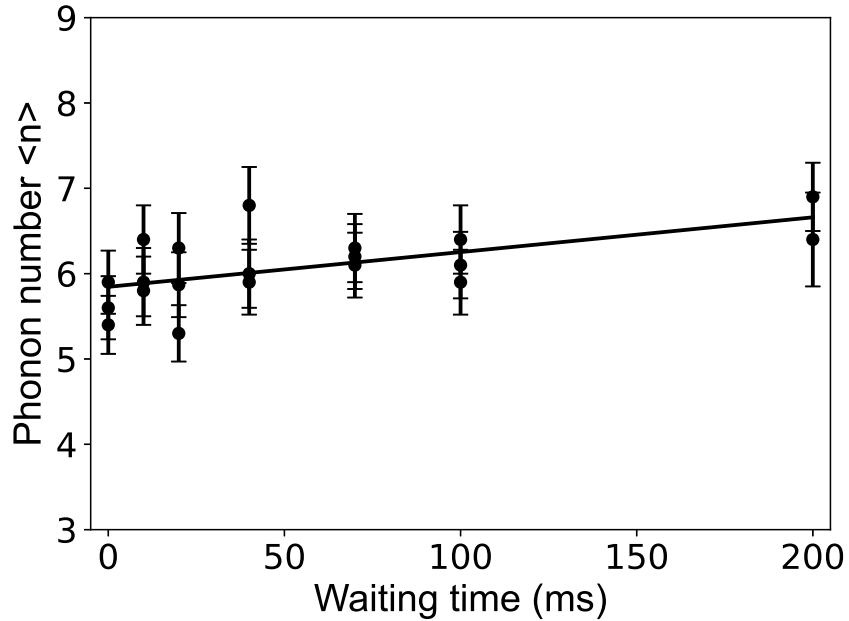


Figure 9: Heating rate of axial motional mode. The mean phonon number is measured for different waiting times after PGC. A linear fit reveals a heating rate of 4.1(8) phonons per second for a trap frequency of  $2\pi \times 285\text{kHz}$ .

## 6 Conclusion and outlook

We implement three-dimensional polarization gradient cooling for trapped  $\text{Ca}^+$  ions in a linear Paul trap with initial temperatures far outside the Lamb-Dicke regime. Sideband spectroscopy after PGC shows all motional modes to be well below the Doppler-cooling limit. Efficient cooling close to the ground state even with elevated initial phonon numbers ( $> 4000$  phonons) or substantial residual micromotion demonstrates the robustness of the presented method. We demonstrated PGC for single ions and extended the cooling technique to linear crystals consisting of up to four ions reaching a final mean phonon number of  $12.5(7)$  at the axial trap frequency of  $2\pi \times 190$  kHz. Furthermore, we find that the spectral impurity of the laser field affects the cooling rate and cooling limit of PGC. Thus, we employ a Fabry-Pérot cavity to suppress amplified spontaneous emission of the diode laser. The mean phonon number is improved by  $2.0(3)$  phonons and the cooling time is decreased by a factor of  $2.1(2)$ . A mean phonon number limit of  $5.4(4)$  is achieved at a trap frequency of  $2\pi \times 285$  kHz in the axial direction. The heating rate of the trap is estimated to be  $4.1(8)$  phonons per second at this trap frequency, indicating a possible lower limit to the achievable phonon number. The cavity-filter technique provides an option to improve PGC, even with diode lasers, whose spectrum contains an ASE component. Robust PGC can be beneficial for capturing and sympathetically cooling injected "impurity" ions, e.g. thorium[38], below the Doppler cooling limit.

## 7 Acknowledgements

WL thanks M. K. Joshi for helpful discussions. We thank Ulrich Poschinger and Daniel Wessel for careful reading and helpful comments. This work was supported in part by the Cluster of Excellence "Precision Physics, Fundamental Interactions, Structure of Matter" (PRISMA+ EXC 2118/1) and Helmholtz Excellence Network ExNet020, funded by the German Research Foundation (DFG) within the German Excellence Strategy (Project ID 39083149), the DFG Reinhart Koselleck project and the Deutsche Forschungsgemeinschaft (DFG, German Research Foundation) – Project-ID 429529648 – TRR 306 QuCoLiMa ("Quantum Cooperativity of Light and Matter"). WL thanks for the financial support by the "China-Germany Postdoctoral Exchange Program".

## References

- [1] Zhang J, Pagano G, Hess P W, Kyprianidis A, Becker P, Kaplan H, Gorshkov A V, Gong Z X, and Monroe C 2017 *Nature* **551** 601–604
- [2] Blatt R and Roos C F 2012 *Nat. Phys.* **8** 277–284
- [3] Johanning M, Braun A, Timoney N, Elman V, Neuhauser W, and Wunderlich C 2009 *Phys. Rev. Lett.* **102** 073004–4
- [4] Hilder J, Pijn D, Onishchenko O, Stahl A, Orth M, Lekitsch B, Rodriguez-Blanco A, Müller M, Schmidt-Kaler F and Poschinger U 2021 *arXiv* **2107** 06368–8
- [5] Blatt R and Wineland D 2008 *Nature* **453** 1008–1015
- [6] Cirac J I and Zoller P 1995 *Phys. Rev. Lett.* **74** 4091–4094
- [7] Brewer S M, Chen J S, Hankin A M, Clements E R, Chou C W, Wineland D J and Hume D B 2019 *Phys. Rev. Lett.* **123** 033201–6
- [8] Keller J, Burgermeister T, Kalincev D, Didier A, Kulosa A, P, Nordmann T, Kiethe J, and Mehlstäubler T E 2019 *Phys. Rev. A* **99** 013405–12
- [9] Huang Y, Guan H, Liu P L, Bian W, Ma L S, Liang K, Li T C, and Gao K L 2016 *Phys. Rev. Lett.* **116** 013001–6
- [10] Chou C W, Hume D B, Koelemeij J C, Wineland D J, and Rosenband T 2010 *Phys. Rev. Lett.* **104** 070802–4
- [11] Pyka K, Keller J, Partner H L, Nigmatullin R, Burgermeister T, Meier D M, Kuhlmann K, Retzker A, Plenio M B, Zurek W H, del Campo A and Mehlstäubler T E 2013 *Nat. Commun.* **4** 2291–6
- [12] Roos C F, Chwalla M, Kim K, Riebe M, and Blatt R 2006 *Nature* **443** 316–319
- [13] Nägerl H C, Roos C F, Leibfried D, Rohde H, Thalhammer G, Eschner J, Schmidt-Kaler F, and Blatt R 2000 *Phys. Rev. A* **61** 023405–9
- [14] Clark C R, Goeters J E, Dodia Y K, Viteri C R and Brown K R 2010 *Phys. Rev. A* **81** 043428–7
- [15] William D. Phillips 1998 *Rev. Mod. Phys.* **70** 721–741
- [16] Chalony M, Kastberg A, Klappauf B and Wilkowski D 2011 *Phys. Rev. Lett.* **107** 243002–5

- [17] Eeschner J, Morigi G and Schmidt-Kaler F 2003 *J. Opt. Soc. Am. B* **20** 1003–1015
- [18] Diedrich F, Bergquist J C, Itano W M and Wineland D J 1989 *Phys. Rev. Lett.* **62** 403–406
- [19] Poulsen G, Miroshnychenko Y and Drewsen M 2012 *Phys. Rev. A* **86** 051402–4
- [20] Goodwin J F, Stutter G, Thompson R C and Segal D M 2016 *Phys. Rev. Lett.* **116** 143002–5
- [21] Che H, Deng K, Xu Z T, Yuan W H, Zhang J and Lu Z H 2017 *Phys. Rev. A* **96** 013417–9
- [22] Seck C M, Kokish M G, Dietrich M R and Odom B C 2016 *Phys. Rev. A* **93** 053415–10
- [23] Thompson J D, Tiecke T G, Zibrov A S, Vuletić V and Lukin M D 2013 *Phys. Rev. Lett.* **110** 133001–5
- [24] Feng L, Tan W L, De A, Menon A, Chu A, Pagano G and Monroe C 2020 *Phys. Rev. Lett.* **125** 053001–5
- [25] Roos C F, Leibfried D, Mundt A, Schmidt-Kaler F, Eschner J and Blatt R 2000 *Phys. Rev. Lett.* **85** 5547–5550
- [26] Lechner R, Maier C, Hempel C, Jurcevic P, Lanyon B P, Monz T, Brownnutt M, Blatt R and Roos C F 2016 *Phys. Rev. A* **93** 053401–10
- [27] Qiao M, Wang Y, Cai Z, Du B, Wang P, Luan C, Chen W, Noh H R and Kim K 2021 *Phys. Rev. Lett.* **126** 023604–6
- [28] Cohen-Tannoudji C N and Phillips W D 1990 *Phys. Today* **43** 33–40
- [29] Cohen-Tannoudji C N 1998 *Rev. Mod. Phys.* **70** 707–719
- [30] Wineland D J, Dalihard J and Cohen-Tannoudji C N 1992 *J. Opt. Soc. Am. B* **9** 32–42
- [31] S. Chu 1991 *Science* **253** 861–866
- [32] Dalihard J and Cohen-Tannoudji C N 1989 *J. Opt. Soc. Am. B* **6** 2023–2045
- [33] Cirac J I, Blatt R, Parkins A S and P. Zoller 1993 *Phys. Rev. A* **48** 1434–1445
- [34] Yoo S M and Javanainen J 1993 *Phys. Rev. A* **48** R30–4
- [35] G. Birkl and J. A. Yeazell and R. Rückerl and H. Walther 1994 *Europhys. Lett.* **27** 197–202
- [36] Ejtemaee S and Haljan P C 2017 *Phys. Rev. Lett.* **119** 043001–6
- [37] Joshi M K, Fabre A, Maier C, Brydges T, Kiesenhofer D, Hainzer H, Blatt R and Roos C F 2020 *New J. Phys.* **22** 103013–15
- [38] Groot-Berning K, Stopp F, Jacob G, Budker D, Haas R, Renisch D, Runke J, Thörle-Pospiech P, Düllmann C E and Schmidt-Kaler F 2019 *Phys. Rev. A* **99** 023420–6
- [39] Stopp F, Groot-Berning K, Jacob G, Budker D, Haas R, Renisch D, Runke J, Thörle-Pospiech P, Düllmann C E and Schmidt-Kaler F 2019 *Hyperfine interact.* **240** 33–10
- [40] Haas R, Kieck T, Budker D, Düllmann C E, Groot-Berning K, Li W, Renisch D, Schmidt-Kaler F, Stopp F and Viatkina A 2020 *Hyperfine interact.* **241** 25–8
- [41] Seiferle B, Lars von der Wense, Bilous P V, Amersdorffer I, Lemell C, Libisch F, Stellmer S, Schumm T, Düllmann C E, Pálffy A and Thierolf P G 2019 *Nature* **573** 243–246